Macromolecules
ARTICLE

Macromolecules **2010**, *43*, 10123–10131 **10123**
DOI: 10.1021/ma1021677

Long Wavelength Concentration Fluctuations and Cage Scale Ordering of Nanoparticles in Concentrated Polymer Solutions

So Youn Kim,[†] Lisa M. Hall,[†,∥] Kenneth S. Schweizer,[†,‡,§] and Charles F. Zukoski*[,†,‡,§]

[†]*Department of Chemical and Biomolecular Engineering,* [‡]*Department of Materials Science, and* [§]*Frederick Seitz Materials Research Laboratory, University of Illinois, Urbana, Illinois 61801, United States.* [∥] *Present address: Sandia National Laboratories, Albuquerque, New Mexico 87185, United States.*

Received September 17, 2010; Revised Manuscript Received November 3, 2010

ABSTRACT: Ultrasmall-angle X-ray scattering is employed to probe the local and long wavelength collective structure of ternary mixtures of silica nanoparticles suspended in concentrated solutions of polyethyleneglycol in the good solvent ethanol. In the dilute polymer limit, these suspensions are stabilized via electrostatic repulsions, at intermediate polymer concentrations the nanoparticles aggregate, while in the polymer melt limit they again become homogeneous due to the formation of thermodynamically stable discrete adsorbed polymer layers on the nanoparticles. Solvent dilution of the polymer melt is found to modify the nanoparticle concentration fluctuations on all length scales in a manner that can be understood as a monotonic reduction of the favorable polymer−particle interfacial cohesive attraction. The measurements are quantitatively compared with predictions of the two-component Polymer Reference Interaction Site Model theory modified to account in an implicit manner for solvent addition via an effective contact strength of interfacial attraction, ε_{pc}. Good agreement between theory and experiment is found without adjustable parameters based on the idea that ε_{pc} linearly decreases with solvent volume fraction. The joint experimental−theoretical work suggests a new mechanism for restabilization of aggregated particle suspensions at high polymer concentration based on the thermodynamically controlled interface cohesion of weakly adsorbing polymers that contrasts with the classic kinetic repulsive barrier mechanism under nonadsorbing depletion attraction conditions.

I. Introduction

Polymer-colloid mixtures find application in a wide range of products, from coatings and structural composites, to car tires. These applications rely on different degrees of particle dispersion to deliver the desired chemical, mechanical and optical properties. A great deal is understood about suspension phase behavior and degree of particle aggregation when particles are suspended in dilute and semidilute polymer solutions, especially under nonadsorbing conditions where polymers mediate depletion attractions between the colloids.[1,2] The depletion attraction increases in strength with polymer concentration and can induce the formation of discrete particle aggregates, a space-spanning gel, or liquid−liquid phase separation, depending on particle size and volume fraction, and polymer concentration and molecular weight.[1,3−7] Less is understood for adsorbing polymers in suspension, which can drive bridging flocculation or steric stabilization corresponding to polymer-mediated attractive and repulsive forces, respectively[8] or in the case of block copolymers with different strengths of adsorption that can result in ordered and bicontinuous phases.[9] Even less is known about the microstructure and effective interactions of nanoparticles in concentrated polymer solutions or dense melts. Of great interest in the manufacture of polymer nanocomposites are methods to control the degree of dispersion under concentrated polymer solution conditions.[3,4,6,7] Here we investigate nanoparticle structure and osmotic compressibility at polymer concentrations from semidilute up to homopolymer melt densities with particular attention paid to the role of polymer segment-particle surface interactions in controlling how nanoparticles are spatially organized.

Recent theoretical and experimental advances in understanding melt polymer nanocomposites have established that the quantitative strength and spatial range of the polymer segment-particle surface interactions control the qualitative nature of nanoparticle dispersion.[5,10−14] One key prediction is that the degree of aggregation is a nonmonotonic function of the strength of polymer segment-particle contact attraction strength, ε_{pc}. For very small ε_{pc} compared to thermal energy ("dewetting" interface), depletion attractions dominate and nanoparticles aggregate into large compact clusters at nearly all particle volume fractions. For large ε_{pc}, polymers form tight bridges between the nanoparticles resulting in phase separation or perhaps nonequilibrium polymer−particle network formation. But at intermediate ε_{pc}, adsorbed polymer layers form that remain discrete, nonoverlapping, and thermodynamically stable, resulting in a net repulsive interparticle potential-of-mean-force (PMF) between the nanoparticles and mixture stability.[5,10−14] Scattering structure factor and second virial coefficient measurements for melts of silica nanoparticles in polyethyleneglycol (PEG) and polytetrahydrofuran (PTHF) have confirmed the basic features of the theoretical predictions.[5,15]

Here we investigate the effect of solvent (ethanol) dilution on the same 44 nm silica plus PEG (400 MW) mixtures studied previously, which are fully dispersed under melt conditions. If the polymer is diluted by ethanol, the nanoparticles strongly aggregate. Hence, this system shows a re-entrant type of behavior, unstable at lower polymer concentration, but stable at high polymer concentration, a phenomenon often called depletion restabilization that is observed in a variety of experimental systems.[3,6,16] Models for the origin of depletion restabilization

*To whom correspondence should be addressed. E-mail: czukoski@illinois.edu.

Published on Web 11/18/2010

Table 1. Polymer-to-Ethanol Volume Ratios and Nanoparticle Packing Fractions Studied in This Work[a]

PEG to ethanol vol ratio (PEG−EtOH)	R_{PEG}	ϕ_{p0}	ε_{pc}(kT)	particle packing fractions (ϕ_c) (polymer concentration in a unit of weight % of total mixture)						
0.5:0.5	0.5	0.20	0.275	0.05 (54 wt %)	0.10 (51 wt %)		0.20 (45 wt %)	0.30 (40 wt %)	0.35 (37 wt %)	
0.6:0.4	0.6	0.24	0.33		0.10 (61 wt %)	0.15 (58 wt %)	0.20 (54wt)	0.30 (48 wt %)		0.40 (41 wt %)
0.7:0.3	0.7	0.28	0.385	0.05 (75 wt %)	0.10 (71 wt %)	0.15 (67 wt %)	0.20 (63 wt %)	0.30 (55 wt %)	0.35 (51 wt %)	
0.8:0.2	0.8	0.32	0.44		0.10 (81 wt %)	0.15 (76 wt %)	0.20 (71 wt %)	0.30 (63 wt %)		
0.9:0.1	0.9	0.36	0.495	0.05 (96 wt %)	0.10 (91 wt %)	0.15 (86 wt %)	0.20 (81 wt %)	0.30 (71 wt %)		

[a] The quantity ϕ_{p0} denotes the packing fraction of polymer in the region of space not occupied by nanoparticles. To a first approximation, it is the polymer concentration that would exist in a reservoir in equilibrium with the suspension across a membrane that will pass solvent and polymer but not particles.

remain tentative and rely on changes in the range of the depletion attraction as polymer concentration increases above their overlap concentration and polymer adsorption is claimed to induce kinetic barriers to aggregation.[2,4] Here we extend the successful microscopic Polymer Reference Interaction Site Model (PRISM) theory of melt polymer nanocomposites[10−12] to account for solvent addition and address this question of depletion restabilization in the context of equilibrium statistical mechanics. We experimentally and theoretically find that as modest amounts of good solvent are added to the nanocomposite, polymer segments are driven away from the particle surface resulting in decreased stabilization.

In Section II, the experimental methods used to prepare and characterize the polymer−particle solutions are described. Section III presents and discusses experimental structure factors. Microstructural studies are carried out using ultrasmall-angle X-ray scattering on suspensions where particle volume fraction is varied at constant volume ratio of polymer-to-ethanol. This protocol is adopted to mimic, to a first approximation, holding the polymer chemical potential constant as particle volume fraction is raised. Such an approach facilitates consideration of the particles as a pseudo-one component system[17] where the effective particle pair interaction potential is independent of particle volume fraction. In Section IV, we briefly discuss PRISM theory and its extension to the three-component system of present interest focusing mainly on the changes necessary to account for the presence of solvent. Section V compares theory and experiment for the collective nanoparticle structure factors. Conclusions are drawn in Section VI.

II. Experimental System and Methods

A. Sample Preparation. Silica nanoparticles were synthesized based on the method of Stöber et al.[18] using the base-catalyzed hydrolysis and condensation of tetraethylorthosilicate (TEOS). The reaction temperature was 55 °C. A 3610 mL sample of 200 proof ethanol was mixed with 96 mL of deionized water, and 156 mL of ammonium hydroxide was then added as a catalyst. The reaction was allowed to run for ∼3−4 h. After mixing, 156 mL of TEOS was added. This procedure produces nanoparticles of diameter $D = 44 \pm 4$ nm suspended in ethyl alcohol. Particle diameters were determined based on SEM performed on 100 particles yielding a diameter of 43 ± 5 nm; alternatively, fitting of the single particle form factor determined by the angle dependence of X-ray scattering from a dilute suspension of particles yielded a diameter of 43 ± 1 nm.

PEG 400 was purchased from Sigma-Aldrich, and 200 proof ethyl alcohol was supplied from Decon Lab. Inc. As discussed previously,[5] the effective diameter of a PEG monomer is $d \sim 0.6$ nm. The nanoparticle size was chosen to minimize the size asymmetry ratio, D/d but have a large enough particle such that small-angle X-ray scattering can be used to probe both long wavelength and cage scale collective concentration fluctuations.

After particle synthesis, the alcosol was concentrated approximately 10 times by heating in a ventilation hood. During this process, the excess of ammonium hydroxide was removed. For the preparation of polymer suspensions, the exact mass of each component (silica, PEG400, ethanol) was determined to create the desired particle and polymer concentrations. In this process, the initial volume fraction of particles is required. Particle volume fractions were calculated using the masses of each component and their densities. The silica particle density is 1.6 g/cm^3.[15] The defined mass of alcosol is then mixed with the defined mass of PEG 400. Samples were heated in a vacuum oven to drive off ethanol. The vacuum oven was purged several times with nitrogen followed by evacuation of the chamber to remove oxygen that degrades PEG at high temperature.[19] Once the ethanol was evaporated, the necessary amount of ethanol was added to the sample and fully mixed on the vortex mixer to produce the desired concentrations of particles and PEG.

PEG 400 is a liquid at room temperature and is completely miscible with ethanol ($T_{m,PEO400} = 8$ °C). In the absence of PEG, the alcosol appears transparent blue. As the silica and PEG have nearly identical refractive indices ($n_{silica} = 1.4555$, $n_{PEG} = 1.4539$), the polymer/particle mixture becomes increasingly transparent as polymer concentration is increased. In the absence of ethanol, the polymer nanocomposite melt is fully transparent, and this index matching greatly reduces (nearly eliminates) van der Waals attractions between silica particles thereby rendering them model hard spheres.[15] In the absence of polymer, particle surface charge is implicated as a source of stability through large positive second virial coefficients that drop rapidly upon addition of soluble electrolyte. Increasing polymer concentration rapidly decreases the particle charge such that at the polymer concentrations studied here, there is no evidence of particle charge in particle second virial coefficients or particle microstructure at elevated volume fractions.[20]

Polymer concentration will be described in terms of the parameter R_{PEG}, defined as the ratio of the polymer volume to the polymer plus solvent volume. For $0.05 < R_{PEG} < 0.45$, we find the nanoparticles slowly aggregate. For $R_{PEG} < 0.05$ or $R_{PEG} > 0.45$, the suspensions are observed to be stable and well dispersed. Table 1 lists the experimental values of R_{PEG} explored in this study.[20]

B. Side-Bounce Ultrasmall Angle X-ray Scattering (SBUSAXS). SBUSAXS experiments were conducted at the X-ray operations and Research beamline on the 32ID-B at the Advanced Photon Source (APS), Argonne National laboratory. The instrument employs a Bonse-Hart camera and Si(111) optics, which extends the q-range to scattering vectors as small as 2×10^{-3} Å^{-1}. Additional side-reflection Si(111) stages enables effective pinhole collimation that reduces slit smearing to a minimum. An absolute calibration converts the scattering intensity from

counts per second to absolute units of cm^{-1} based knowledge of the sample thickness along the beam path. Samples were loaded in multiposition holders supplied by the beamline scientist. The sides of each cell chamber in the holders were sealed with two Kapton polyimide slides. All measurements were performed at room temperature. Measurements on each sample took about 30 min including loading and experiments. The background intensity, measured every fifth sample, was subtracted from the total scattering intensity. The background scattering intensity at each polymer concentration was negligible compared to the scattering by the particles (the background intensity from ethanol differs from 90 wt % PEG solution only by a factor of 10^{-13} cm^{-1}, while the scattering intensity of the sample with silica particles is of order 10^{-3} cm^{-1}).

After subtraction of the scattering of the corresponding polymer solution in absence of the particles, the measured scattering was considered to arise only from the silica nanoparticles thereby enabling use of the effective one-component model.[15] The X-ray scattering intensity from a single component material can be written as

$$I(q,\phi_c) = \phi_c V_c \Delta\rho_e{}^2 P(q) S(q,\phi_c) + B \quad (1)$$

where ϕ_c is the nanoparticle packing fraction, $\Delta\rho_e$ is the excess electron scattering length density of the particles relative to the PEG solution phase, V_c is the particle volume, $P(q)$ is the single particle form factor, $S(q,\phi_c)$ is the collective nanoparticle structure factor (normalized to unity at large q), and B is the background scattering amplitude. For spheres of diameter D, the form factor is

$$P(q) = \left(3\frac{\sin\left(\frac{qD}{2}\right) - \left(\frac{qD}{2}\right)\cos\left(\frac{qD}{2}\right)}{\left(\frac{qD}{2}\right)^3} \right)^2 \quad (2)$$

Moderate nanoparticle polydispersity is taken into account using a Gaussian diameter distribution to calculate an average form factor given by

$$\overline{P}(q) = \frac{\int \frac{1}{\sqrt{2\pi}\nu} e^{(-D_c - \overline{D}_c)^2/2\nu^2)} D_c{}^6 P(q) \mathrm{d}D_c}{\int \frac{1}{\sqrt{2\pi}\nu} e^{(-D_c - \overline{D}_c)^2/2\nu^2)} D_c{}^6 \mathrm{d}D_c} \quad (3)$$

Fitting the experimental form factor to the experimental data yields a standard deviation in size of $0.07\overline{D}_c$.

III. Experimental Structure Factors

We have made many measurements of the nanoparticle structure factor under the conditions summarized in Table 1. In this section, we present representative examples and discuss the key trends in qualitative physical terms.

Figure 1 shows the change in scattering intensity with increasing particle volume fraction at a fixed R_{PEG} ratio of 0.9. The intensity plots result from a convolution of scattering from single particles and correlations of particle centers-of-mass. We note that in the polymer concentration range studied, the solutions are clear and transparent indicating almost perfect index of refraction matching. Thus, we expect that van der Waals attractions between the nanoparticles are effectively suppressed. As the nanoparticle volume fraction grows, the low q intensity generally decreases due to reduced osmotic compressibility of the particle subsystem, while a peak of increasing intensity emerges on the cage ($qD \sim 2\pi$) scale associated with local nanoparticle spatial order.

Collective nanoparticle structure factors were obtained by dividing the scattering intensity from the concentrated particle

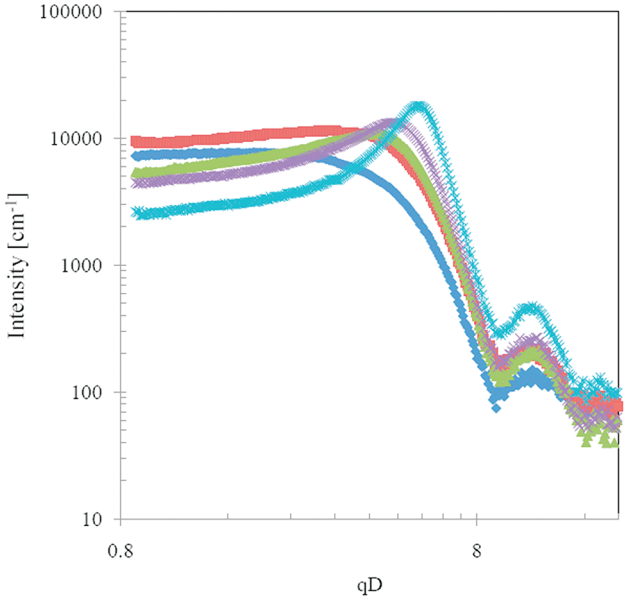

Figure 1. Experimental scattered intensity versus dimensionless wavevector at fixed polymer: ethanol volume ratio $R_{PEG} = 0.9$ and $\phi_c = 0.05$ (blue diamond), 0.10 (red square), 0.15 (green triangle), 0.20 (lavender X), and 0.30 (aqua asterisk).

suspension by its dilute limit analog (ds) at the same polymer concentration

$$S(q,\phi_c) = \frac{I(q,\phi_c)}{I_{ds}(q,\phi_c)} \frac{\phi_{c,ds}}{\phi_c} \quad (4)$$

In the dilute particle limit, $S(q) = 1$. Structure factors are extracted under high polymer concentration conditions where the nanoparticles are stable (miscible homogeneous phase). Particle packing fractions from 0.05 to 0.4 have been studied at a fixed R_{PEG} (see Table 1). For example, when $R_{PEG} = 0.6$ with $\phi_c = 0.10$, 10% of the total sample volume is occupied by the silica particles and the remaining 90% is polymer and ethanol. Since the ratio of PEG to ethanol volumes is fixed at 3:2, the volume fraction of polymer in the mixture is 0.54, while the volume fraction of ethanol is 0.36. As ϕ_c is increased at $R_{PEG} = 0.6$, the polymer concentration based on total suspension mass decreases such that as ϕ_c changes from 0.1 to 0.4, and the polymer concentration drops from 61 to 41 wt %.

All experimental structure factors are liquidlike in the sense of showing a plateau value at low qD with a wide angle, amorphous fluidlike peak that grows in magnitude and moves to larger qD as volume fraction is raised. For the studied experimental conditions, the silica particles show no signs of aggregation as would be indicated by upturns in $S(q)$ as $q \to 0$.

The structure factors corresponding to the scattering intensities in Figure 1 are shown in Figure 2 based on $\phi_{c,ds} = 0.05$. For this low solvent concentration sample, three monotonic trends with particle volume fraction emerge that are typical of all our data. (1) The low wavevector amplitude strongly decreases corresponding to the nanoparticle subsystem becoming less compressible. (2) The wide angle peak at $q = q^*$ shifts from $q^*D \sim 4$ to $q^*D \sim 6$ corresponding to a shorter length scale of local cage order. This trend follows since $2\pi/q^*D$ is a measure of the mean distance between a central particle and its first nearest neighbor shell. (3) The cage peak intensity, $S(q^*)$, initially increases very weakly and then strongly grows for the more concentrated particle mixtures implying greater coherence of the cage scale packing. The behavior shown in Figure 2 is typical of all R_{PEG} values studied. Our quantitative analysis, including comparison

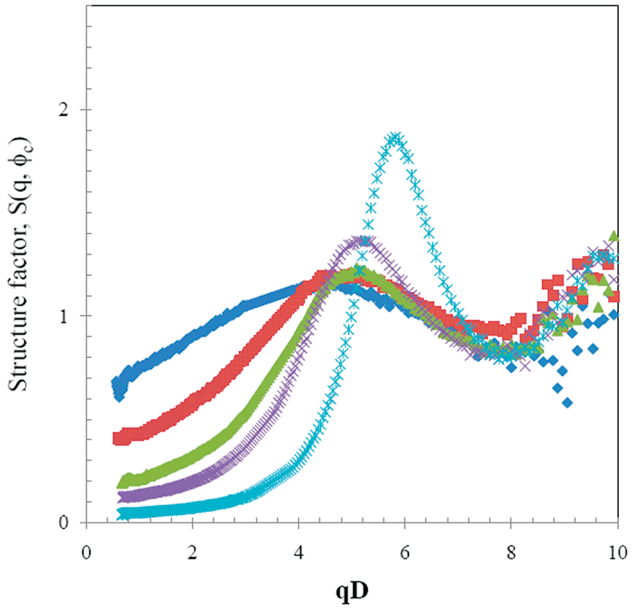

Figure 2. Experimental particle structure factor versus wavevector at $R_{PEG} = 0.9$ and ϕ_c of 0.05 (blue diamond), 0.10 (red square), 0.15 (green triangle), 0.20 (lavender X), and 0.30 (aqua asterisk).

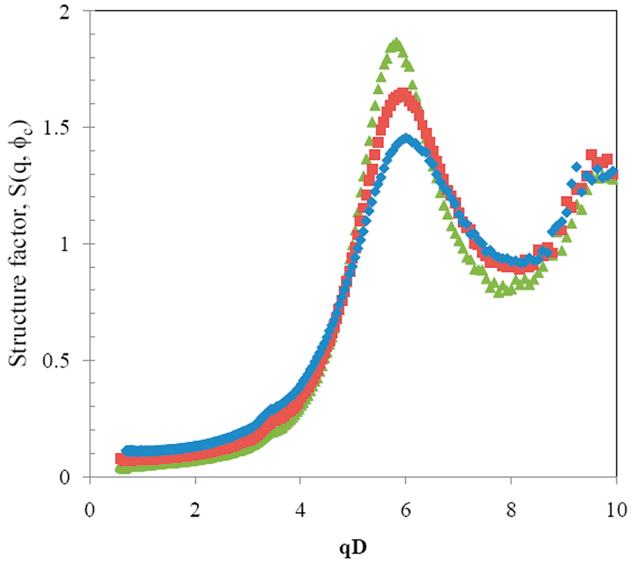

Figure 3. Experimental particle structure factors versus wavevector at a particle packing fraction of 0.30 and varying polymer−ethanol volume ratio $R_{PEG} = 0.9$ (green triangle), 0.7 (red square), and 0.5 (blue diamond).

with theory, in Section IV will focus on how these three features systematically evolve as a function of polymer-to-solvent ratio and particle volume fraction.

Figure 3 shows an example of how the nanoparticle collective structure factor changes with polymer−solvent ratio at a fixed, high particle packing fraction of 0.3. As solvent replaces polymer (decreasing R_{PEG}) in the concentrated solution regime, the inverse dimensionless osmotic compressibility, $1/S(0)$, decreases significantly, the peak position shifts slightly to higher wavevectors, and the peak intensity strongly decreases. Physically, these three trends are largely a consequence of solvent reducing the degree of nanoparticle ordering, on both local and global length scales, or equivalently that the nanoparticles experience stronger effective repulsions as R_{PEG} increases. Although the particle packing fraction is fixed, the consequences of solvent dilution on the intensity at $q \sim 0$, and on the cage scale, "look like" how the structure of a one-component particle fluid changes if its volume packing is reduced. However, such a picture would imply the location of the cage peak would decrease with solvent dilution. This is not the case experimentally, which is one indication of the more complex structural rearrangements that occur in a ternary mixture and is qualitatively consistent with the theoretically motivated idea that as more good solvent is added the amount of adsorbed polymer, and the corresponding effective steric layer thickness, decreases.

IV. Theory and Model

A. Background. PRISM theory has been extensively applied to dense polymer nanocomposites.[10−14] Recently it was extended to account for the expected increase in total system packing fraction with the addition of hard nanoparticles to a polymer melt composed of small monomers that can approximately fill the interstitial space between nanoparticles at the pure polymer melt density.[5] Here we further extend this model to the case of variable bulk polymer packing fraction when the suspending medium is a polymer solution. The solvent will be treated implicitly by reducing the polymer packing fraction and adjusting the polymer adsorption strength, roughly in the spirit of an effective mean field chi-parameter and effective (but compressible) two-component mixture model.[21]

PRISM theory[22] as implemented here consists of three coupled nonlinear integral equations[5,11−14] for the site−site intermolecular pair correlation functions, $g_{ij}(r)$, where i and j refer to polymer monomer (p) or nanoparticle (c).[10−14] The nanoparticles are hard spheres of diameter D, and the polymer is a freely jointed chain (FJC) composed of N identical spherical interaction sites. The single chain structure factor in Fourier space is[22]

$$\omega_p(k) = [1 - f^2 - 2N^{-1}f + 2N^{-1}f^{N+1}]/(1-f)^2 \qquad (5)$$

where $f = \sin(kl)/(kl)$, and the persistence length $l = 4/3d$ (typical of flexible polymers).[3,17] The generalized Ornstein−Zernike, or Chandler-Andersen,[23] matrix integral equations relate $g = 1 + h$ to $\mathbf{C}$ in Fourier space as[22]

$$\mathbf{H}(k) = \Omega(k)\mathbf{C}(k)[\Omega(k) + \mathbf{H}(k)] \qquad (6)$$

where the diagonal matrix $\Omega(k)$ contains the elements $\rho_i\omega_i(k)\delta_{ij}$, $\mathbf{C}(k)$ consists of the elements $C_{ij}(k)$, and $\mathbf{H}(k)$ is composed of the elements $\rho_i\rho_j h_{ij}(k)$, where $h_{ij}(r) = g_{ij}(r) - 1$. The number densities are $\rho_p = \phi_p/(d^3\pi/6)$ and $\rho_c = \phi_c/(D^3\pi/6)$, where ϕ_p and ϕ_c are the polymer and particle packing fractions, respectively, as discussed in more detail below.

The site−site Percus−Yevick closure approximation is used for polymer−polymer (p-p) and polymer−nanoparticle (p-c) correlation functions, while the hypernetted chain (HNC) closure is used for the nanoparticle−nanoparticle correlation function[11]

$$C_{ij}(r) = (e^{-U_{ij}(r)} - 1)(1 + h_{ij}(r) - C_{ij}(r)) \qquad (7)$$

$$C_{cc}(r) = -U_{cc}(r) + h_{cc}(r) - \ln g_{cc}(r) \qquad (8)$$

This specific model and version of PRISM theory has been previously developed and compared with experiment, only for dense melt polymer−particle mixtures. Possible swelling of polymer chains in a good solvent is not taken into account. However, in our present applications, the polymers are short and hence intrachain excluded volume effects are expected to be very weak.[24] Moreover, we focus on the concentrated

polymer solution regime which further minimizes conformational nonideality effects.

In eqs 7 and 8, U_{ij} are the pair decomposable site−site potentials, where U_{cc} and U_{pp} are taken to be purely hard core. The chemical nature of the mixture enters solely via the two parameters of an attractive monomer-particle interfacial attraction: the strength at contact ε_{pc} (in units of thermal energy) and spatial range α (in units of the monomer diameter). Beyond the hard core distance of closest approach, the exponential interfacial potential is given by

$$U_{pc}(r) = -\varepsilon_{pc} \exp\left(\frac{-\left(r-\frac{(D+d)}{2}\right)}{\alpha d}\right) \quad (9)$$

Henceforth, all lengths (energies) are expressed in units of the monomer diameter (thermal energy). The key parameter ε_{pc} describes the effective energetics of transferring a polymer segment from a particle-free solution to being adsorbed on the nanoparticle surface. As such, it implicitly depends on the material-specific cohesive interactions among the polymer, solvent, and nanoparticle. In all calculations reported below, the degree of polymerization is taken to be $N = 100$, the size asymmetry ratio $D/d = 10$, and the spatial range of attraction is $\alpha = 0.5$. These are typical values as motivated in prior work[5,11−14] and have been shown to result in PRISM theory predictions for nanoparticle structure factors in good agreement with experiment for the silica-PEG melt mixture.[5]

An inexact Newton's method is employed to numerically solve the coupled nonlinear PRISM integral equations, which yield the real space pair correlation functions, $g_{ij}(r)$. The polymer and nanoparticle collective partial structure factors then follow as

$$\mathbf{S}'(k) = \mathbf{\Omega}(k) + \mathbf{H}(k) = (\mathbf{I} - \mathbf{\Omega}(k)\mathbf{C}(k))^{-1}\mathbf{\Omega}(k) \quad (10)$$

where $\mathbf{I}$ is the identity matrix and $\mathbf{S}'$ is the dimensionalized version of $\mathbf{S}$, $S'_{ii} = \rho_i S_{ii}$.

As nanoparticles are added to the mixture, the total packing fraction is increased such that the theoretical polymer packing fraction outside the volume excluded by nanoparticles remains constant[25] at ϕ_{p0}

$$\phi_t = \phi_c + \phi_{p0}\left(1 - \phi_c\left(1 + \left(\frac{d}{D}\right)\right)^3\right) \quad (11)$$

In eq 11, the suspension is considered of fixed total volume. When a fixed volume of particles is added, a volume of polymer solution at concentration ϕ_{p0} must be removed. The term in brackets in eq 11 accounts for the reduction in number of polymer segment number when that volume is removed. Calculations based on it for polymer−particle melts have been shown to agree well with experimental scattering profiles over a wide range of particle packing fractions and under both weak and intermediate strength interfacial cohesion conditions.[5]

To summarize, the above set of equations can be numerically solved to determine the microstructure of a nanoparticle−polymer mixture as described in detail in ref 5. Originally developed for particles in a polymer melt, we have here extended the theoretical approach to account for variable polymer density due to solvent. Of particular interest in the present work is the effect of reducing ϕ_{p0}.

B. Effect of Solvent Dilution. Previously we have investigated the effects of varying ε_{pc} through changes in polymer chemistry at ϕ_{p0} fixed at the melt polymer density.[5] For example, PTHF, which is known to weakly adsorb on silica, was shown to have a lower interfacial strength ($\varepsilon_{pc} = 0.35$) than PEG ($\varepsilon_{pc} = 0.55$). In this work we explore the effects of changing ϕ_{p0} on mixture microstructure and particle stability. One of our key findings is that adding solvent may allow a simple means to adjust the effective ε_{pc} and thus provide a new method to process nanocomposites and cast films. In principle, dilute polymers in a good solvent will adsorb less strongly (or not at all) to nanoparticle surfaces compared with those in the dense melt since there is an additional free energy penalty for a segment to leave the good solvent environment and contact the particle surface. The solvent used here, ethanol, is chemically similar to the polymer monomers, as each are composed of two saturated carbons and an oxygen. Ignoring the chemical differences between the hydroxyl group of ethanol and the ether group of PEG as a first approximation, the major difference between the monomer and solvent is size. A segment of the FJC model is a sphere of diameter d which represents several (∼3) PEG monomers,[5] each approximately the size, of ethanol. Because of its smaller size, and for simplicity, ethanol is represented only implicitly (continuum solvent model). Therefore, the polymer packing fraction is lowered as solvent is added. Specifically, the initial polymer concentration, ϕ_{p0}, that enters eq 11 is calculated from the volume fraction of polymer in the polymer/solvent mixture, R_{PEG}, which remains constant as particles are added, and the polymer melt packing fraction $\phi_{p0,m}$, as

$$\phi_{p0} = R_{PEG}\phi_{p0,m} \quad (12)$$

In the experiment, mixtures are created with fixed R_{PEG} and fixed ϕ_{p0}, but increasing ϕ_c as shown in Table 1. The theoretical melt packing fraction $\phi_{p0,m} = 0.40$, as used in previous studies,[5] which yields a realistic dimensionless isothermal compressibility of a pure polymer melt of $S_{pp}(q = 0) \sim 0.2$.

The key material parameter is the polymer segment-nanoparticle attractive contact strength, ε_{pc}, the absolute value of which controls the aggregation state.[5,10−14] For intermediate ε_{pc} values, thermodynamically stable "bound polymer layers" form around nanoparticles, resulting in a miscibility window in the phase diagram such that in melts the nanoparticles are stable and fully dispersed at all particle volume fractions. Because the monomers are represented as hard spheres and the solvent is implicit, the interfacial attraction strength ε_{pc} actually represents the overall enthalpic gain of transferring a monomer from the continuous suspending phase to the particle surface. Reference 5 found $\varepsilon_{pc} = 0.55$ for the PEG melt and silica based on quantitative comparisons of theory and experiment for the nanoparticle collective structure factor. If the adsorbed monomer originates from a polymer−solvent mixture, the relevant enthalpic considerations upon its placement near the particle surface are loss of polymer−solvent interactions (strength ε_{ps}), loss of nanoparticle−solvent interactions (strength ε_{cs}), and gain of solvent−solvent interactions (strength ε_{ss}). The former two occur with frequency proportional to the fraction of solvent ($1 - R_{PEG}$), while the latter is proportional to $(1 - R_{PEG})^2$. Hence, we propose a simple mean-field-like estimate of the effective interfacial attraction strength as

$$\varepsilon_{pc,effective} = \varepsilon_{pc,melt} - (1 - R_{PEG})\varepsilon_{ps} - (1 - R_{PEG})\varepsilon_{cs} + (1 - R_{PEG})^2\varepsilon_{ss} \quad (13)$$

Equation 13 is reminiscent of the dilution approximation for the χ-parameter of a ternary solvent plus a AB polymer blend,[21] allowing for the possibility of solvent selectivity.

For our system, the solvent is chemically similar to the monomer. Hence, interactions with itself and with the monomer are modeled per an athermal good solvent ($\varepsilon_{ps} = \varepsilon_{ss} = 0$), and interaction with the nanoparticle is the same as that of the monomer ($\varepsilon_{cs} = \varepsilon_{pc,melt}$). Under these specific conditions, eq 13 becomes

$$\varepsilon_{pc,effective} = R_{PEG}\varepsilon_{pc,melt} = 0.55R_{PEG} \qquad (14)$$

This simple zeroth order model has no adjustable parameters. The polymer−nanoparticle effective interfacial attraction strength decreases linearly to zero with polymer/solvent ratio (R_{PEG}). The physical picture is that the addition of good solvent reduces the tendency for polymer adsorption, which ultimately results in such a small effective ε_{pc} that depletion attraction and/or unshielding of the van der Waals attraction due to dielectric constant changes results in nanoparticle aggregation. The calculated ε_{pc} for each polymer-to-solvent ratio are given in Table 1.

As further motivation for the applicability of this model to our experimental system, we note that it is known there is a favorable adsorption energy for ethanol on silica surfaces.[26−28] Experiment indicates that PEG400 adsorbs to the silica surfaces out of ethanol with an affinity that is an order of magnitude smaller than adsorption out of water.[20] This implies that the polymer−particle attraction strength in dilute solution is much smaller than in the melt. By assuming a simple linear relationship between $\varepsilon_{pc,effective}$ and solvent concentration, and that the $\varepsilon_{pc,effective}$ is negligible in the dilute limit, we again obtain eq 14.

C. Sample Theoretical Results. In the theoretical model, solvent dilution is accounted for by reducing both the polymer packing fraction and changing the effective interfacial adsorption strength using eqs 12 and 14. To investigate the relative and absolute importance of these two effects of solvent dilution, we first implement them separately.

Previously we showed that in a polymer melt, stable (dispersed) nanoparticle microstructures were well captured by the theory. Specifically, the three distinguishing features of the predicted and measured collective nanoparticle structure factors were quantitatively compared: the height, $S(q^*)$ and location, q^*, of the wide angle cage peak, and the nanoparticle osmotic compressibility $S(0)$. With decreasing ε_{pc}, $S(0)$ increases, and the particle cage scale peak decreases in intensity and shifts to higher wavevector.[5] As a result, measuring $S(q)$ over a range of wave vectors and particle volume fractions provided a set of internally consistent checks for the determination of the crucial material parameter ε_{pc}. This comparison showed that all three measures of the microstructure are well described by an ε_{pc} that is independent of particle volume fraction. In addition, ε_{pc} was found to vary with polymer chemistry.[5] For example, at fixed particle packing fraction, ε_{pc} decreases when the silica nanoparticle is transferred from the more strongly adsorbing PEG melt to the more hydrophobic PTHF melt. As ε_{pc} decreases, the PTHF system is predicted to move closer to depletion phase separation. Indeed while PEG nanocomposite melts were stable at all volume fractions, above a critical volume fraction the PTHF nanocomposite melts are observed to exhibit strong aggregation and ultimately gelation.

In the present work we extend these studies to explore the effects of decreasing polymer concentration via solvent dilution. Theoretically we do this in two steps. First we assume ε_{pc} is independent of ϕ_{p0}. Second, we explore changes in microstructure when ε_{pc} is varied with ϕ_{p0} as in eq 14.

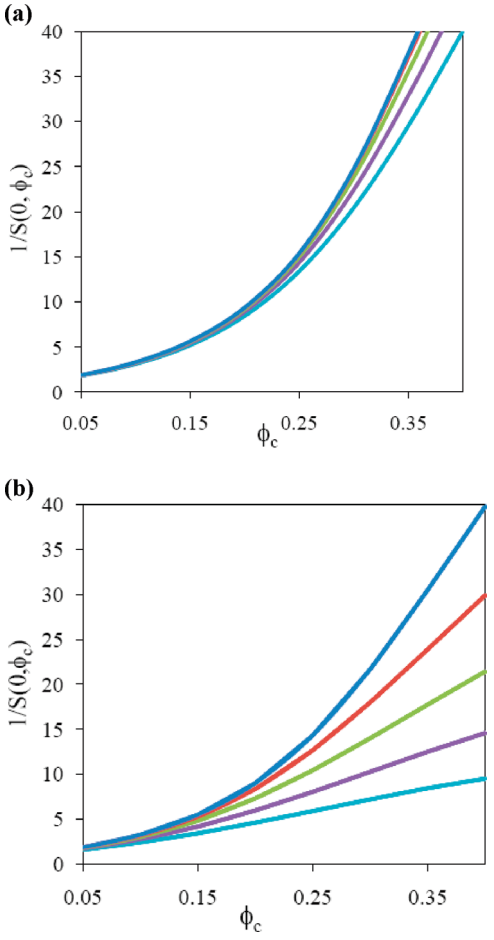

Figure 4. PRISM predictions for the inverse osmotic compressibility as a function of particle packing fraction (ϕ_c) with varying R_{PEG} at (a) fixed $\varepsilon_{pc} = 0.55$ and (b) adjusted ε_{pc} as shown in Table 1. For both (a) and (b), R_{PEG} are 0.9, 0.8, 0.7, 0.6, and 0.5 from top to bottom.

Figure 4 shows representative theoretical calculations of the inverse of the nanoparticle osmotic compressibility as a function of nanoparticle packing fraction as R_{PEG} is decreased from 0.9 to 0.5 for (a) a fixed $\varepsilon_{pc} = 0.55$, and (b) a diluted ε_{pc} given in eq 14. At constant $\varepsilon_{pc} = 0.55$, decreasing R_{PEG} only slightly increases $S(0)$. However, if both R_{PEG} and ε_{pc} decrease then $S(0)$ increases far more, although the increase is still less than that due to lowering ε_{pc} at constant $R_{PEG} = 1$ (not shown, but reported in ref 5). Reduction of the local polymer density close to nanoparticles drives depletion attraction, so it is physically reasonable that decreasing the amount of polymer has little effect in the miscible regime but a much greater effect at low ε_{pc} and serves to push the system further from strong depletion behavior resulting in an upturn of $S(0)$ at low wavevectors. The experimental trends for $S(0)$ in Figure 3 suggest the particles experience enhanced repulsion as R_{PEG} increases, qualitatively as predicted in Figure 4b if ε_{pc} increases with R_{PEG}.

V. Comparison of Experiment and Theory

We now analyze experimentally and theoretically the three characteristic features of $S(q)$ discussed in Section III over a wide range of R_{PEG} and ϕ_c. The packing fraction dependencies of $1/S(0)$, $S(q^*D)$ and q^*D are shown in Figures 5, 6, and 7, respectively, for $R_{PEG} = 0.5, 0.6, 0.7, 0.8, 0.9$. The results confirm the observations in Figure 3 namely that, for all volume fractions, as the polymer concentration is increased at fixed ϕ_c three observations are made: (i) long wavelength density fluctuations are

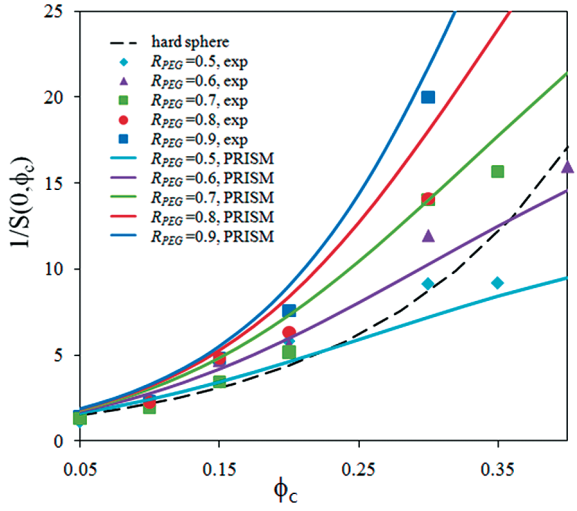

Figure 5. Experimental inverse osmotic compressibilities ($1/S(0,\phi_c)$) as a function of particle packing fraction (ϕ_c) at various R_{PEG}. The corresponding PRISM predictions are plotted as solid curves. The reference hard sphere fluid result is also shown (dashed curved).

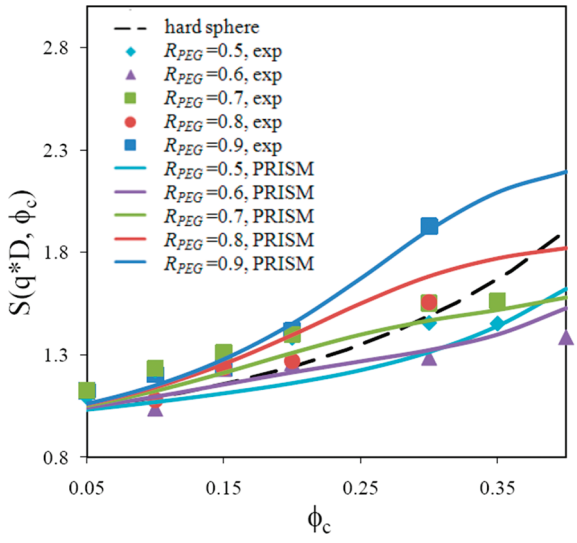

Figure 6. Experimental height of the cage peak of the particle structure factor ($S(q^*D,\phi_c)$) as a function of particle packing fraction (ϕ_c) at various R_{PEG}. The corresponding PRISM are plotted as solid curves. The reference hard sphere fluid result is also shown (long dashed).

suppressed ($S(0)$ decreases), (ii) coherency of the cage scale order increases ($S(q^*)$ increases), and (iii) the position of the cage peak is a weak function of R_{PEG}, with no obvious trend.

At fixed R_{PEG}, Figures 5 and 6 show that the growth of $1/S(0)$ and $S(q^*)$, respectively, with volume fraction becomes weaker as the amount of solvent present grows, with subtle exceptions at lower R_{PEG} values. Also shown in Figures 5 and 6 are predictions assuming the particles are hard spheres in a vacuum at the same packing fractions as the nanoparticles in the polymer solution. Comparing the reference hard sphere and experimental results, one sees that while the presence of polymer increases $1/S(0)$ for all R_{PEG} at low volume fractions suggesting enhanced repulsions due to the presence of polymer, at high volume fractions and at low R_{PEG} values the experimental values fall below the analogous hard sphere behavior indicating enhanced long wavelength concentration fluctuations over those of the analogous hard sphere fluid. Nanoparticle cage coherency, as quantified by the magnitude of $S(q^*)$, shows similar trends; at large values of R_{PEG}, the particle cages are better defined (more order) that expected from

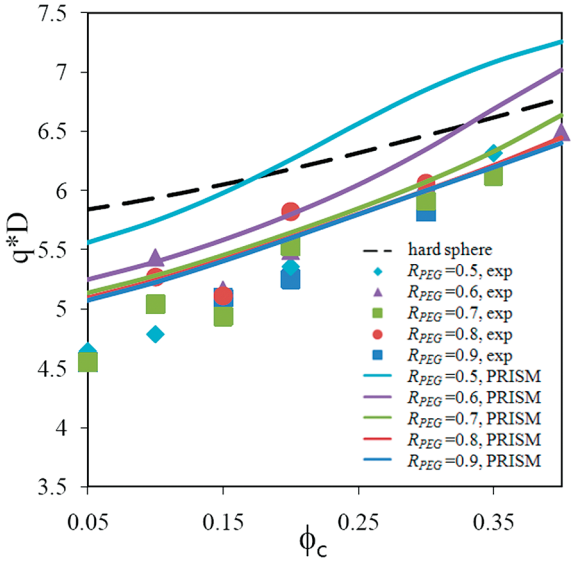

Figure 7. Experimental normalized wavevector at the cage peak of the particle structure factor, q^*D, as a function of particle packing fraction (ϕ_c). The corresponding PRISM predictions are plotted as solid curves. The reference hard sphere fluid result is also shown (dashed curved).

the analogous hard sphere fluid, while at low R_{PEG} the cages are less well-defined than expected for hard spheres suggesting diminished repulsions relative to the hard sphere reference. Hence, to summarize, at high R_{PEG} the strongly adsorbed polymer layer results in a significantly lower nanoparticle compressibility and increased cage scale ordering compared to the hard sphere fluid analog, but at lower R_{PEG} polymer adsorption is reduced resulting in depletion attraction and hence (at $R_{PEG} = 0.5$) both $1/S(0)$ and $S(q^*)$ fall below that of the reference hard sphere fluid. These differences in behavior of the hard sphere fluid reference system and nanocomposite clearly demonstrate the important role of polymer and solvent on the nanoparticle scattering features. Figure 7 reinforces this conclusion since in all cases the experimental q^* data fall below the reference hard sphere fluid curve indicating that the silica nanoparticles order on a larger length scale than bare hard spheres in a vacuum at the same volume fraction, consistent with steric repulsion between adsorbed polymers on the particle surfaces.

A detailed comparison of the experimental data with theory is also shown in Figures 5-7 based on the linear variation of ε_{pc} with R_{PEG} model of eq 14. Recall there are no adjustable parameters in the theoretical calculations. Overall, the measured and theoretically predicted trends agree qualitatively, if not quantitatively. Figure 5 shows PRISM theory predicts that with increasing solvent dilution $S(0)$ increases by an amount that is in good agreement with experiment for all values of ϕ_c studied. Recall that the analogous constant ε_{pc} model PRISM results in Figure 4a are very different and disagree with experiment. This strongly suggests that the decrease in effective ε_{pc} (as opposed to entropic depletion effects of dilution) is the main driver of the nanoparticle structural changes upon solvent addition.

The theory also compares well to experimental results for cage peak height $S(q^*)$, as seen in Figure 6. At low ϕ_c the peak height is small, and the experimental trend versus R_{PEG} is unclear, while the theory predicts a slight decrease in peak height with solvent addition. At intermediate and high nanoparticle volume fractions, both experiment and theory show decreasing local order as R_{PEG} decreases from 0.9 to 0.6. At the lowest $R_{PEG} = 0.5$, this trend reverses experimentally with a slightly higher $S(q^*)$ than observed for $R_{PEG} = 0.6$. Interestingly, at high ϕ_c the analogous PRISM theory results also shows this small increase in $S(q^*)$. Again, the agreement of parameter free comparisons of PRISM

and the experimental data is qualitatively excellent and nearly quantitatively accurate over a wide range of R_{PEG} and particle volume fraction.

Figure 7 compares theoretical and experimental values of the dimensionless wavevector of the primary cage peak. As seen in the experimental data, the theoretical results for $R_{PEG} > 0.6$ also show q^* is smaller than that of the reference hard sphere fluid. Moreover, q^* varies approximately linearly with ϕ_c, as observed experimentally. At the lowest polymer concentrations, as ϕ_c increases the theoretical q^* increases above that of pure hard spheres. This is perhaps due to the decreasing amount of adsorbed polymer as ε_{pc} becomes small, and the resulting tendency of particles to aggregate. For the experimental data, q^* remains nearly constant regardless of R_{PEG} and is smaller than the theoretical result suggesting that the extent of adsorbed layer polymer-mediated repulsions are a bit larger than captured in the model. Note all values of q^* in the presence of ethanol are larger than observed in melts at all measured volume fractions (as reported in Figure 5 of ref 5), again indicating the greater polymer-mediated repulsive interactions at higher polymer concentrations, an effect that is captured by the theory.

Collectively, the results in Figures 5-7 demonstrate that the no adjustable parameter predictions of PRISM theory for the structural consequences of solvent dilution are quite accurate, essentially as good as found previously for the melt nanocomposite.[5] Moreover, the combined experimental and theoretical results demonstrate that with increasing polymer concentration the nanoparticles are stabilized via the formation of adsorbed polymer layers. This physical picture is at odds with the naïve application of depletion potential concepts where increased polymer solution concentration will produce increased strengths of attraction between the particles.[1,29−32] Hence, we suggest a new mechanism for polymer-induced restabilization based on the formation of thermodynamically stable and discrete adsorbed polymer layers when the effective monomer-particle attraction strength is modest (of order kT). At a more detailed level, PRISM theory suggests the increased stability arises from two factors. First, the van der Waals attraction between nanoparticles are essentially eliminated due to index matching at polymer concentrations greater than $R_{PEG} = 0.5$.[20] As a result, in the pseudo two-component mixture of particles and polymer, the direct particle interactions are primarily volume exclusion. Second, with increased polymer concentration there is an increased effective enthalpic attraction between the polymer and nanoparticle which drives more segmental adsorption thereby creating larger repulsive steric interactions and increased particle stability.

The experiments described here have been designed to approximately hold the polymer chemical potential constant as particle concentration is increased. Such an approximate pseudo-one-component model is often invoked to treat a suspension as composed of particles interacting with a volume fraction independent PMF.[17] In applying the effective two-component PRISM theory, we relax this view by explicitly accounting for the polymeric species. Our results suggest that at fixed polymer chemical potential ε_{pc} is independent of particle volume fraction, thereby restoring its microscopic nature.

VI. Summary

In a recent combined experiment-theory study, Anderson and three of us performed a quantitative analysis of the effects of changing polymer chemistry and adsorption strength on the collective nanoparticle structure factor under dense melt conditions.[5] It was shown that PRISM theory accurately describes the microstructural features based solely on the chemically specific value of the interfacial attraction strength ε_{pc}. In the present study, we have explored the effect of adding a good solvent, ethanol, to the PEG-silica mixture, as a function of nanoparticle volume fraction and the polymer-to-solvent volume ratio in the concentrated polymer solution regime. The experimental scattering results compare well with the no adjustable parameter PRISM theory calculations based on the simple idea that solvent dilution simultaneously modifies the polymer packing fraction and effective interfacial attraction strength. More broadly, our results demonstrate that measurement of nanoparticle concentration fluctuations in dense polymer solutions and melts, in conjunction with microscopic theory, can be used as an in situ tool for extracting the strength of particle−polymer segment attraction.

The key new finding discussed in this paper is the strong nanoparticle microstructural changes that occur upon variation of monomer−nanoparticle attraction strength, ε_{pc}, via solvent dilution of the melt mixture. We emphasize the discovered structural changes are not universal since ε_{pc} depends on the chemistry of the polymer and particle as well as the solvent−solvent and solvent−nanoparticle interactions. However, our results do suggest a practical method for manipulating ε_{pc}. As a result, one can imagine processing conditions where nanoparticles are stabilized during processing by driving polymer to the particle surface through the addition of an antisolvent that is later removed resulting in nanoparticles trapped in a dispersed state. Poor solvent conditions may also be interesting in creating conditions where ε_{pc} increases to a point of triggering the formation of polymer−nanoparticle bridging complexes as predicted theoretically.[10−12] Finally, the generalization of the PRISM approach to explicitly treat solvent molecules is a worthy future goal.

Acknowledgment. SBUSAXS data was collected at the 32ID-B at the Advanced Photon Source (APS), Argonne National Laboratory. The APS is supported by the U.S. Department of Energy, Office of Science, Office of Basic Energy Sciences, under Contract No. DE-AC02-06CH11357. This work was supported by the Nanoscale Science and Engineering Initiative of the National Science Foundation under NSF Award DMR-0642573.

References and Notes

(1) Poon, W. C. K. *J. Phys.: Condens. Matter* **2002**, *14*, R859.
(2) Russel, W. B.; Saville, D. A.; Schowalter, W. R. *Colloidal Dispersions*; Cambridge University Press: Cambridge, UK, 1989.
(3) Dutta, N.; Green, D. *Langmuir* **2008**, *24*, 5260–5269.
(4) Feigin, R. I.; Napper, D. H. *J. Colloid Interface Sci.* **1980**, *75*, 525–541.
(5) Hall, L. M.; Anderson, B. J.; Zukoski, C. F.; Schweizer, K. S. *Macromolecules* **2009**, *42*, 8435–8442.
(6) Huang, H.; Ruckenstein, E. *Langmuir* **2006**, *22*, 4541–4546.
(7) Semenov, A. N. *Macromolecules* **2008**, *41*, 2243–2249.
(8) Surve, M.; Pryamitsyn, V.; Ganesan, V. *J. Chem. Phys.* **2006**, 125.
(9) Anderson, J. A.; Sknepnek, R.; Travesset, A. *Phys. Rev. E* **2010**, *82* (2), 021803.
(10) Hall, L. M.; Jayaraman, A.; Schweizer, K. S. *Curr. Opin. Solid State Mater. Sci.* **2010**, *14*, 38–48.
(11) Hall, L. M.; Schweizer, K. S. *J. Chem. Phys.* **2008**, *128*, 23.
(12) Hooper, J. B.; Schweizer, K. S. *Macromolecules* **2005**, *38*, 8858–8869.
(13) Hooper, J. B.; Schweizer, K. S. *Macromolecules* **2006**, *39*, 5133–5142.
(14) Hooper, J. B.; Schweizer, K. S. *Macromolecules* **2007**, *40*, 6998–7008.
(15) Anderson, B. J.; Zukoski, C. F. *Macromolecules* **2007**, *40*, 5133–5140.
(16) Sharma, A.; Tan, S. N.; Walz, J. Y. *J. Colloid Interface Sci.* **1997**, *190*, 392–407.
(17) Lekkerkerker, H. N. W.; Poon, W. C. K.; Pusey, P. N.; Stroobants, A.; Warren, P. B. *Europhys. Lett.* **1992**, *20*, 559–564.
(18) Stober, W.; Fink, A.; Bohn, E. *J. Colloid Interface Sci.* **1968**, *26*, 62.
(19) Mkhatresh, O. A.; Heatley, F. *Polym. Int.* **2004**, *53*, 1336–1342.
(20) Kim, S. Y. Master's Thesis, University of Illinois at Urbana-Champaign, Urbana, IL, 2009.

(21) Fredrickson, G. H. *The Equilibrium Theory of Inhomogeneous Polymers*; Oxford University Press: New York, 2005.
(22) Schweizer, K. S.; Curro, J. G. Integral equation theories of the structure, thermodynamics, and phase transitions of polymer fluids. In *Advances in Chemical Physics*; Wiley and Sons: New York, 1997; Vol. *98*, pp 1−142.
(23) Chandler, D.; Anderson, H. C. *J. Chem. Phys*. **1972**, *57*, 1930.
(24) Rubinstein, M.; Colby, R. H. *Polymer Physics*; Oxford: New York, 2003.
(25) Biben, T.; Hansen, J. P. *Phys. Rev. Lett*. **1991**, *66*, 2215–2218.
(26) Evans, D. F.; Wennerström, H. *The Colloidal Domain: Where Physics, Chemistry, Biology, and Technology Meet*; VCH: Cambridge, 1994.
(27) Kawaguchi, M.; Hada, T.; Takahashi, A. *Macromolecules* **1989**, *22*, 4045–4047.
(28) Kawaguchi, M.; Sakakida, K. *Macromolecules* **1990**, *23*, 4477–4479.
(29) Ramakrishnan, S.; Fuchs, M.; Schweizer, K. S.; Zukoski, C. F. *J. Chem. Phys*. **2002**, *116*, 2201–2212.
(30) Ramakrishnan, S.; Fuchs, M.; Schweizer, K. S.; Zukoski, C. F. *Langmuir* **2002**, *18*, 1082–1090.
(31) Shah, S. A.; Chen, Y. L.; Ramakrishnan, S.; Schweizer, K. S.; Zukoski, C. F. *J. Phys.: Condens. Matter* **2003**, *15*, 4751–4778.
(32) Shah, S. A.; Chen, Y. L.; Schweizer, K. S.; Zukoski, C. F. *J. Chem. Phys*. **2003**, *118*, 3350–3361.